 CMC, vol.29, no.1, pp.75-101, 2012

MLPG Analysis of Layered Composites with Piezoelectric and Piezomagnetic Phases

J. Sladek[1], V. Sladek[1], S. Krahulec[1], M. Wünsche[2] and Ch. Zhang[2]

Abstract: A meshless method based on the local Petrov-Galerkin approach is proposed, to solve static and dynamic problems of two-layered magnetoelectroelastic composites with specific properties. One layer has pure piezoelectric properties and the second one is a pure piezomagnetic material. It is shown that the electric potential in the piezoelectric layer is induced by the magnetic potential in the piezomagnetic layer. The magnetoelectric effect is dependent on the ratio of the layer thicknesses. Functionally graded material properties of the piezoelectric layer and homogeneous properties of the piezomagnetic layer are considered too. The magnetoelectric composites are analyzed under a pure magnetic or combined magneto-mechanical load. Various boundary conditions and geometric parameters are considered to analyze their influence on the value of the electromagnetic parameter.

Keywords: Meshless local Petrov-Galerkin method (MLPG), moving least-squares approximation, magnetoelectric effect, bilayer mutifferoic composite, size effect

1 Introduction

An important application of composite structures is the use of the product property, which is found in the composite structures but is absent in the individual phases (Ryu et al., 2002). It has been observed that remarkably larger magnetoelectric (ME) effect is observed for composites than for either composite constituent (Nan, 1994; Feng and Su, 2006). Smith et al. (1985) and Shaulov et al. (1989) found that the piezocomposites can provide a higher piezoelectric strain modulus d_{31} than the constituents. Numerical results by Dunn (1993) showed that the effective thermal expansion coefficients of composites could significantly exceed those of the matrix and the fiber phases.

[1] Institute of Construction and Architecture, Slovak Academy of Sciences, 84503 Bratislava, Slovakia, sladek@savba.sk

[2] Department of Civil Engineering, University of Siegen, D-57068 Siegen, Germany

Originally, sintered granular composites were used for producing composite magnetoelectric (ME) effects. The ME is defined as the ratio between the magnetic (electrical) field output over the electrical (magnetic) input. The ME effect was discovered in 1894 by Curie. The ME coupling coefficient in single-phase compounds is small for principle reasons (Eerenstein et al., 2006). However, the ME effect is intensively studied to utilize it for the energy conversion between the magnetic and electric fields and the ME memory elements, smart sensors and transducers (Wood and Austin, 1975; Wang et al., 2005). From earlier investigations it is well known that some composite materials can provide superior properties compared to their virgin monolithic constituent materials. Similarly one can expect larger ME effect in layered composites than in monoliths. An applied magnetic field induces strain in the magnetostrictive constituent of the bilayer mutifferoic composite. This is passed on to the piezoelectric constituent, where it induces an electric polarization. In turn an applied electric field induces a magnetization via the mechanical coupling between the constituents. A strong ME effect has been recently observed by Pan and Wang (2009) in artificially fabricated multiferroic composites. It has been shown that the ME response of the laminated composites is determined by four major aspects: (i) the magnetic, electrical and mechanical coefficients of the constituents; (ii) the respective thickness and number of the piezoelectric and magnetostrictive layers; (iii) the type of boundary constituents; (iv) the orientation of the constituents and of the applied electric or magnetic fields. The influence of the thickness ratio for piezomagnetic and piezoelectric layers h_m/h_e on the ME effect was investigated in other papers too (Shastry et al., 2004, Laletin et al., 2008, Zhai et al., 2004).

A noticeable enhancement of the ME response is to make use of strong internal electromagnetic fields by finding components with a large dielectric or magnetic susceptibility. The largest dielectric coefficients are found in ferroelectrics, while ferromagnets display the largest magnetic permeabilities. Consequently, ferromagnetic ferroelectrics are primary candidates for displaying giant ME effects. Subsequently it was discovered that the coupling between the constituents can be greatly enhanced by using laminated double, triple or multilayer composites. Theories for understanding the interaction between the constituents in both bulk and laminated composites have been developed, and it has been shown that the efficiency of the micromechanical coupling plays a crucial role. A micromechanical model to predict the effective moduli of multicoated elliptic fibrous composites of piezoelectric and piezomagnetic phases is given by Kuo (2011).

All aspects of research works on composite ME effects discussed thus far were accompanied or preceded by intense theoretical works with the intention of understanding the coupling between the composite phases and quantifying the result-

ing ME response. The pioneering experiments on the ME were given by Van den Boomgard *et al*, (1974, 1976). The early works were mainly devoted to the description of ME coupling mechanisms in bulk composites. In the simplest case the effective linear ME effect of a composite made of two isotropic materials was determined from the ME constants of the constituents and the dielectric and magnetic permeabilities of the constituents and the composite (Milgrom and Shtrikman, 1994).

Because of the complex nature of the ME interaction between the constituents the relation between the applied magnetic field and the voltage induced in the detection circuit is not simply linear as in the case of single-phase compounds. Due to the hysteretic nature of the ME effect, the composites may find applications in memory devices. The linear ME effect has a positive or a negative sign, depending on the annealing conditions (parallel or antiparallel magnetic and electric fields). In binary data storage devices the ME material can thus store information in two different states distinguished by the sign of the ME response. Such a memory will be an effective 'read only' memory, since the reading can be done at very high frequencies. Data writing is more difficult because it involves temperature annealing in magnetic and electric fields or the use of very high writing fields (Ryu et al. 2002). Further applications include magnetic field sensors. The transduction properties of the ME effect can also be employed in ME recording heads and electromagnetic pick-ups. Historical perspective, status and future of multiferroic magnetoelectric composites are given in a review paper (Nan et al., 2008).

In the present paper the meshless local Petrov-Galerkin (MLPG) method is developed to investigate the magnetoelectric coupling in bilayered piezomagnetic/piezoelectric composites with various geometrical sizes and boundary conditions. A meshless method based on the local Petrov-Galerkin approach is proposed, to solve two-dimensional (2-D) boundary value problems for layered magnetoelectroelastic composites. The coupled governing partial differential equations are satisfied in a weak-form on small fictitious subdomains (Atluri et al., 2003, Sladek et al., 2008a,b). Nodal points are spread on the analyzed domain, and each node is surrounded by a small circle for simplicity. A Heaviside step function as the test functions is applied in the weak-form on the local subdomains. The local integral equations are derived. The spatial variations of the displacements, electrical and magnetic potentials are approximated by the Moving Least-Squares (MLS) scheme (Atluri, 2004, Belytschko et al., 1996). Numerical techniques based on the C^1-continuity, such as in the present meshless methods, are expected to be more accurate than the conventional discretization techniques for homogeneous or continuously nonhomogeneous solids. However, higher order continuity of primary fields (displacements, electrical and magnetic potentials) would not yield jumps for

secondary fields (gradients of primary fields), if the interface were not modeled. Such jumps occur due to the discontinuities of the material parameters on the interfaces of the joint laminates and the continuity of tractions and electrical/magnetic fluxes. Therefore, a special treatment for modeling discontinuities in piecewise homogeneous solids is required in the case of higher order modeling like in the present meshless approximations. After performing the spatial integrations, one obtains a system of ordinary differential equations. The Houbolt finite-difference scheme (Houbolt, 1950) is applied to the approximation of the time evolution of the field variables.

The proposed MLPG method is applied in several numerical calculations of the magnetoelectric effect for bilayer piezomagnetic/piezoelectric composites. Both static and dynamic loading conditions are considered. The influences of various mechanical boundary conditions and volume ratio of piezomagnetic and piezoelectric constituents on the ME coefficient are investigated.

2 Basic equations

Two-layered composite with only piezoelectric (PE) and only piezomagnetic (PM) properties in each layer exhibits non-vanishing magnetoelectric properties as a whole. This is so because in the PM layer the external magnetic field generates certain strains and due to mechanical contact between the two layers these strains give rise to an electric field in the PE layer. Strictly speaking the evaluation of the magnetoelectric coefficients is a rather complex problem requiring an iterative solution. Only in the first approximation, we can consider the coupling between the PE and PM layers with assuming vanishing magnetoelectric coefficients in each layer. The electric and magnetic boundary conditions for such simplified problems are shown in Fig. 1 for the longitudinal ME effect and the in-plane longitudinal ME effect.

The general constitutive equations for magnetoelectroelastic solids (Nan, 1994) can be written as

$$\sigma_{ij}(\mathbf{x},\tau) = c_{ijkl}(\mathbf{x})\varepsilon_{kl}(\mathbf{x},\tau) - e_{kij}(\mathbf{x})E_k(\mathbf{x},\tau) - d_{kij}(\mathbf{x})H_k(\mathbf{x},\tau), \tag{1}$$

$$D_j(\mathbf{x},\tau) = e_{jkl}(\mathbf{x})\varepsilon_{kl}(\mathbf{x},\tau) + h_{jk}(\mathbf{x})E_k(\mathbf{x},\tau) + \alpha_{jk}(\mathbf{x})H_k(\mathbf{x},\tau), \tag{2}$$

$$B_j(\mathbf{x},\tau) = d_{jkl}(\mathbf{x})\varepsilon_{kl}(\mathbf{x},\tau) + \alpha_{kj}(\mathbf{x})E_k(\mathbf{x},\tau) + \gamma_{jk}(\mathbf{x})H_k(\mathbf{x},\tau), \tag{3}$$

where $\{\varepsilon_{ij}, E_i, H_i\}$ is the set of secondary field quantities (strains, intensity of electric field, intensity of magnetic field) which are expressed in terms of the gradients of the primary fields such as the elastic displacement vector, potential of electric field, and potential of magnetic field $\{u_i, \psi, \mu\}$, respectively. Finally, the elastic

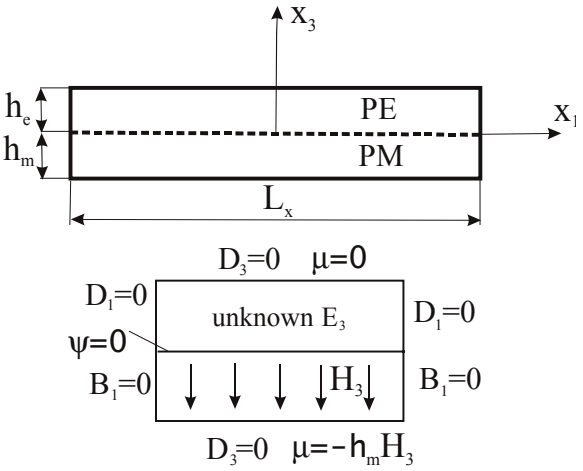

The out-of-plane longitudinal ME effect

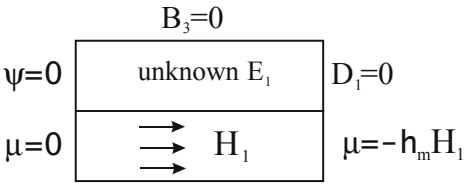

The in-plane longitudinal ME effect

Figure 1: Two-layered multifferoic composite

stress tensor, electric displacement, and magnetic induction vectors $\{\sigma_{ij}, D_i, B_i\}$ form the set of fields conjugated with the secondary fields $\{\varepsilon_{ij}, E_i, H_i\}$. The constitutive equations correlate these two last sets of fields in continuum media including the multifield interactions. The constitutive equations (1)-(3) involve general magnetoelectroelastic interactions in media with spatially dependent material coefficients in continuously non-homogeneous solids. In this paper, we shall consider also functionally graded material properties for one layer (piezomagnetic or piezoelectric) of the two-layered multiferroic composite.

For a layered PE/PM composite where each layer is either piezoelectric (PE) or piezomagnetic (PM), the extended constitutive matrix is reduced to

$$\Lambda_{PE} = \begin{bmatrix} c & e & 0 \\ e^T & h & 0 \\ 0 & 0 & \gamma \end{bmatrix}, \tag{4}$$

$$\Lambda_{PM} = \begin{bmatrix} c & 0 & d \\ 0 & h & 0 \\ d^T & 0 & \gamma \end{bmatrix} \tag{5}$$

for the PE and PM layers, respectively.

The strain tensor ε_{ij} is related to the displacements u_i by

$$\varepsilon_{ij} = \frac{1}{2}\left(u_{i,j} + u_{j,i}\right). \tag{6}$$

The material parameters c_{ijkl}, h_{jk} and γ_{jk} are the elasticity coefficients, dielectric permittivities and magnetic permeabilities, while e_{kij}, d_{kij} and α_{jk} are the piezoelectric, piezomagnetic and magnetoelectric coefficients, respectively.

In the case of some crystal symmetries, one can formulate also the plane-deformation problems (Parton and Kudryavtsev, 1988). For the poling direction along the positive x_2-axis the constitutive equations (1)-(3) are reduced to the following matrix forms

$$\begin{bmatrix} \sigma_{11} \\ \sigma_{33} \\ \sigma_{13} \end{bmatrix} = \begin{bmatrix} c_{11} & c_{13} & 0 \\ c_{13} & c_{33} & 0 \\ 0 & 0 & c_{44} \end{bmatrix} \begin{bmatrix} \varepsilon_{11} \\ \varepsilon_{33} \\ 2\varepsilon_{13} \end{bmatrix} - \begin{bmatrix} 0 & e_{31} \\ 0 & e_{33} \\ e_{15} & 0 \end{bmatrix} \begin{bmatrix} E_1 \\ E_3 \end{bmatrix} - \begin{bmatrix} 0 & d_{31} \\ 0 & d_{33} \\ d_{15} & 0 \end{bmatrix} \begin{bmatrix} H_1 \\ H_3 \end{bmatrix} =$$

$$= \mathbf{C} \begin{bmatrix} \varepsilon_{11} \\ \varepsilon_{33} \\ 2\varepsilon_{13} \end{bmatrix} - \mathbf{L} \begin{bmatrix} E_1 \\ E_3 \end{bmatrix} - \mathbf{K} \begin{bmatrix} H_1 \\ H_3 \end{bmatrix}, \tag{7}$$

$$\begin{bmatrix} D_1 \\ D_3 \end{bmatrix} = \begin{bmatrix} 0 & 0 & e_{15} \\ e_{31} & e_{33} & 0 \end{bmatrix} \begin{bmatrix} \varepsilon_{11} \\ \varepsilon_{33} \\ 2\varepsilon_{13} \end{bmatrix} + \begin{bmatrix} h_{11} & 0 \\ 0 & h_{33} \end{bmatrix} \begin{bmatrix} E_1 \\ E_3 \end{bmatrix} + \begin{bmatrix} \alpha_{11} & 0 \\ 0 & \alpha_{33} \end{bmatrix} \begin{bmatrix} H_1 \\ H_3 \end{bmatrix} =$$

$$= \mathbf{G} \begin{bmatrix} \varepsilon_{11} \\ \varepsilon_{33} \\ 2\varepsilon_{13} \end{bmatrix} + \mathbf{H} \begin{bmatrix} E_1 \\ E_3 \end{bmatrix} + \mathbf{A} \begin{bmatrix} H_1 \\ H_3 \end{bmatrix}, \tag{8}$$

$$\begin{bmatrix} B_1 \\ B_3 \end{bmatrix} = \begin{bmatrix} 0 & 0 & d_{15} \\ d_{31} & d_{33} & 0 \end{bmatrix} \begin{bmatrix} \varepsilon_{11} \\ \varepsilon_{33} \\ 2\varepsilon_{13} \end{bmatrix} + \begin{bmatrix} \alpha_{11} & 0 \\ 0 & \alpha_{33} \end{bmatrix} \begin{bmatrix} E_1 \\ E_3 \end{bmatrix} + \begin{bmatrix} \gamma_{11} & 0 \\ 0 & \gamma_{33} \end{bmatrix} \begin{bmatrix} H_1 \\ H_3 \end{bmatrix} =$$

$$= \mathbf{R} \begin{bmatrix} \varepsilon_{11} \\ \varepsilon_{33} \\ 2\varepsilon_{13} \end{bmatrix} + \mathbf{A} \begin{bmatrix} E_1 \\ E_3 \end{bmatrix} + \mathbf{M} \begin{bmatrix} H_1 \\ H_3 \end{bmatrix}. \tag{9}$$

The Maxwell's equations have usually a quasi-static character in magneto-electro-elastic problems, which is determined by realistic material coefficients. According to Parton and Kudryavtsev (1988) the Maxwell's equations are reduced to two scalar equations

$$D_{j,j}(\mathbf{x},\tau)-\Pi(\mathbf{x})=0, \tag{10}$$

$$B_{j,j}(\mathbf{x},\tau)=0, \tag{11}$$

where Π is the volume density of free charges.

The remaining vectorial Maxwell's equations in the quasi-static approximation, $\nabla\times\mathbf{E}=0$ and $\nabla\times\mathbf{H}=0$, are satisfied identically if

$$E_j(\mathbf{x},\tau)=-\psi_{,j}(\mathbf{x},\tau), \tag{12}$$

$$H_j(\mathbf{x},\tau)=-\mu_{,j}(\mathbf{x},\tau), \tag{13}$$

where $\psi(\mathbf{x},\tau)$ and $\mu(\mathbf{x},\tau)$ are the electric and magnetic potentials, respectively.

To complete the set of the governing equations, eqs. (10) and (11) need to be supplemented by the balance of momentum

$$\sigma_{ij,j}(\mathbf{x},\tau)+X_i(\mathbf{x},\tau)=\rho\ddot{u}_i(\mathbf{x},\tau), \tag{14}$$

where $\ddot{u}_i,\rho$ and X_i denote the acceleration of the displacements, the mass density and the body force vector, respectively.

The following essential and natural boundary conditions are assumed for the mechanical field

$u_i(\mathbf{x},\tau)=\tilde{u}_i(\mathbf{x},\tau)$, on Γ_u,

$t_i(\mathbf{x},\tau)=\sigma_{ij}n_j=\tilde{t}_i(\mathbf{x},\tau)$, on Γ_t,

where $\Gamma=\Gamma_u\cup\Gamma_t$.

Similarly, we assume for the electrical field

$\psi(\mathbf{x},\tau)=\tilde{\psi}(\mathbf{x},\tau)$, on Γ_p,

$n_i(\mathbf{x})D_i(\mathbf{x},\tau)\equiv Q(\mathbf{x},\tau)=\tilde{Q}(\mathbf{x},\tau)$, on Γ_q,

in which $\Gamma=\Gamma_p\cup\Gamma_q$, and for the magnetic field

$\mu(\mathbf{x},\tau)=\tilde{\mu}(\mathbf{x},\tau)$, on Γ_a,

$n_i(\mathbf{x})B_i(\mathbf{x},\tau)\equiv S(\mathbf{x},\tau)=\tilde{S}(\mathbf{x},\tau)$, on Γ_b,

where $\Gamma=\Gamma_a\cup\Gamma_b$, Γ_u is the part of the global boundary Γ with prescribed displacements, while on Γ_t, Γ_p, Γ_q, Γ_a and Γ_b the traction vector, the electric potential, the normal component of the electric displacement vector, the magnetic potential and

the normal component of the magnetic induction vector are prescribed, respectively. Recall that in dielectric media there are no free electric charges and $\tilde{Q}(\mathbf{x},\tau)$ and $\tilde{S}(\mathbf{x},\tau)$ represent the normal components of the electric displacement vector and the magnetic induction vector, respectively, on the outer side of the boundary (interface).

3 Meshless local Petrov-Galerkin method

In the previous section, the boundary value problem is formulated. Now, we need to solve the problem. For this purpose, we apply the local integral equation method with meshless approximations. The MLPG method constructs a weak-form over the local fictitious subdomains such as Ω_s, which is a small region taken for each node inside the global domain (Sladek et al., 2008a,b). The local subdomains could be of any geometrical shape and size. In the present paper, the local subdomains are taken to be of a circular shape for simplicity. The local weak-form of the governing equations (14) can be written as

$$\int_{\Omega_s} \left[\sigma_{ij,j}(\mathbf{x},\tau) - \rho\ddot{u}_i(\mathbf{x},\tau) + X_i(\mathbf{x},\tau)\right] u^*_{ik}(\mathbf{x})\, d\Omega = 0, \tag{15}$$

where $u^*_{ik}(\mathbf{x})$ is a test function.

Applying the Gauss divergence theorem to the first integral and choosing a Heaviside step function as the test function $u^*_{ik}(\mathbf{x})$ in each subdomain, one obtains the following local integral equations (LIE)

$$\int_{L_s+\Gamma_{su}} t_i(\mathbf{x},\tau)d\Gamma - \int_{\Omega_s} \rho\ddot{u}_i(\mathbf{x},\tau)d\Omega = -\int_{\Gamma_{st}} \tilde{t}_i(\mathbf{x},\tau)d\Gamma - \int_{\Omega_s} X_i(\mathbf{x},\tau)d\Omega, \tag{16}$$

where $\partial\Omega_s$ is the boundary of the local subdomain which consists of three parts $\partial\Omega_s = L_s \cup \Gamma_{st} \cup \Gamma_{su}$ (Atluri, 2004). Here, L_s is the local boundary that is totally inside the global domain, Γ_{st} is the part of the local boundary which coincides with the global traction boundary, i.e., $\Gamma_{st} = \partial\Omega_s \cap \Gamma_t$, and similarly Γ_{su} is the part of the local boundary that coincides with the global displacement boundary, i.e., $\Gamma_{su} = \partial\Omega_s \cap \Gamma_u$.

From the constitutive equations (1), we get the traction vector as

$$t_i(\mathbf{x},\tau) = \left[c_{ijkl}(\mathbf{x})u_{k,l}(\mathbf{x},\tau) + e_{kij}(\mathbf{x})\psi_{,k}(\mathbf{x},\tau) + d_{kij}(\mathbf{x})\mu_{,k}(\mathbf{x},\tau)\right] n_j(\mathbf{x}).$$

Similarly, one can derive the local integral equations corresponding to the governing equations (10) and (11)

$$\int_{L_s+\Gamma_{sp}} Q(\mathbf{x},\tau)d\Gamma = -\int_{\Gamma_{sq}} \tilde{Q}(\mathbf{x},\tau)d\Gamma + \int_{\Omega_s} \Pi(\mathbf{x})d\Omega, \tag{17}$$

$$\int\limits_{L_s+\Gamma_{sa}} S(\mathbf{x},\tau)d\Gamma = -\int\limits_{\Gamma_{sb}} \tilde{S}(\mathbf{x},\tau)d\Gamma, \tag{18}$$

where

$$Q(\mathbf{x},\tau) = D_j(\mathbf{x},\tau)n_j(\mathbf{x}) = \left[e_{jkl}(\mathbf{x})u_{k,l}(\mathbf{x},\tau) - h_{jk}(\mathbf{x})\psi_{,k}(\mathbf{x},\tau) - \alpha_{jk}(\mathbf{x})\mu_{,k}(\mathbf{x},\tau)\right] n_j,$$

$$S(\mathbf{x},\tau) = B_j(\mathbf{x},\tau)n_j(\mathbf{x}) = \left[d_{jkl}(\mathbf{x})u_{k,l}(\mathbf{x},\tau) - \alpha_{kj}(\mathbf{x})\psi_{,k}(\mathbf{x},\tau) - \gamma_{jk}(\mathbf{x})\mu_{,k}(\mathbf{x},\tau)\right] n_j.$$

The MLS is used for the spatial approximation of the field variables employing a number of nodes spread over the domain of influence. According to the MLS (Belytschko et al., 1996) method, the approximation of the primary fields (mechanical displacements, electric and magnetic potentials) can be given as

$$\mathbf{u}^h(\mathbf{x},\tau) = \mathbf{\Phi}^T(\mathbf{x})\cdot\hat{\mathbf{u}} = \sum_{a=1}^{n} \varphi^a(\mathbf{x})\hat{\mathbf{u}}^a(\tau),$$

$$\psi^h(\mathbf{x},\tau) = \sum_{a=1}^{n} \varphi^a(\mathbf{x})\hat{\psi}^a(\tau),$$

$$\mu^h(\mathbf{x},\tau) = \sum_{a=1}^{n} \varphi^a(\mathbf{x})\hat{\mu}^a(\tau), \tag{19}$$

where the nodal values $\hat{\mathbf{u}}^a = (\hat{u}_1^a(\tau),\ \hat{u}_3^a(\tau))^T$, $\hat{\psi}^a(\tau)$ and $\hat{\mu}^a(\tau)$ are fictitious parameters for the displacements, the electric and magnetic potentials, respectively, and $\varphi^a(\mathbf{x})$ is the shape function associated with the node a.

The number of nodes n used for the approximation is determined by the weight function $w^a(\mathbf{x})$. A 4^{th} order spline-type weight function is applied in the present work

$$w^a(\mathbf{x}) = \begin{cases} 1 - 6\left(\frac{d^a}{r^a}\right)^2 + 8\left(\frac{d^a}{r^a}\right)^3 - 3\left(\frac{d^a}{r^a}\right)^4, & 0 \le d^a \le r^a \\ 0, & d^a \ge r^a \end{cases}, \tag{20}$$

where $d^a = \|\mathbf{x} - \mathbf{x}^a\|$ and r^a is the size of the support domain. In the MLS approximation the convergence rates of the solution may depend upon the nodal distance as well as the size of the support domain (Wen and Aliabadi, 2008). It should be noted that a small size of the subdomains may induce a large oscillation in the

nodal shape functions (Atluri, 2004). A necessary condition for a regular MLS approximation is that at least m weight functions are non-zero (i.e. $n \geq m$) for each sample point $\mathbf{x} \in \Omega$. This condition determines the size of the support domain. It is seen that the C^1-continuity is ensured over the entire domain, and therefore the continuity conditions of the tractions, electric displacements and magnetic inductions are satisfied. However, this highly continuous nature leads to difficulties when there is an imposed discontinuity in the secondary fields (strains, electric and magnetic field vectors). Because of the highly continuous trial function which is at least C^1continuous, it is not trivial to simulate jumps in the strain field. Krongauz and Belytschko (1998) introduced a jump shape function for 2-D problems. It is a trial function with a pre-imposed discontinuity in the gradient of the function at the location of the material discontinuity in addition to the MLS approximation. This method is very tedious for curvilinear interfaces. Cordes and Moran (1996) solved also 2-D problems by using Lagrangian multiplier. The method requires a lot of computational effort when the discontinuity is of an arbitrary geometrical shape.

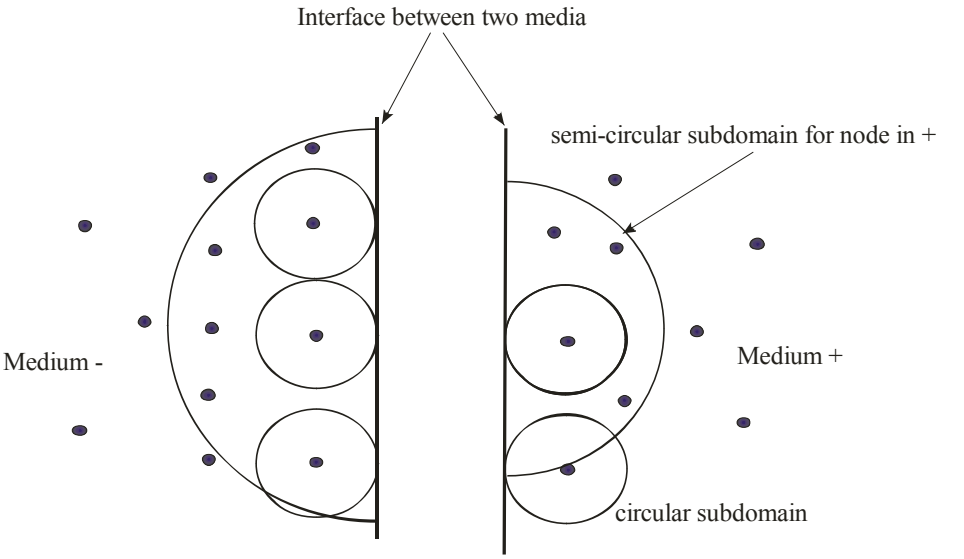

Figure 2: Modeling of material discontinuities

It is much simpler to introduce double nodes to describe the material discontinuity [Sladek et al., 2009]. Two sets of collocation nodes are assigned on both the +side and the –side of the material interface at the same location, but with supporting influence domains lying on corresponding sides of the interface (Fig. 2). In the present paper, we have used this simple and general approach. The MLS

approximations are carried out separately on particular sets of nodes within each of the layers. Then, the support domains for the weights in the weighted MLS-approximations are truncated at the interface of the two media. Therefore, the high order continuity is kept within each layer, but not across their interface. Similarly, the local subdomains considered around nodes are bounded by the interface.

The traction vectors $t_i(\mathbf{x})$ at a boundary point $\mathbf{x} \in \partial\Omega_s$ are approximated in terms of the same nodal values $\hat{\mathbf{u}}^a$, $\hat{\psi}^a$ and $\hat{\mu}^a$ as

$$\mathbf{t}^h(\mathbf{x},\varsigma) = \mathbf{N}(\mathbf{x})\mathbf{C}\sum_{a=1}^{n}\mathbf{B}^a(\mathbf{x})\hat{\mathbf{u}}^a(\tau) + \mathbf{N}(\mathbf{x})\mathbf{L}\sum_{a=1}^{n}\mathbf{P}^a(\mathbf{x})\hat{\psi}^a(\tau) + \mathbf{N}(\mathbf{x})\mathbf{K}\sum_{a=1}^{n}\mathbf{P}^a(\mathbf{x})\hat{\mu}^a(\tau), \tag{21}$$

where the matrices $\mathbf{C}$, $\mathbf{L}$ and $\mathbf{K}$ are defined in eq. (7), the matrix $\mathbf{N(x)}$ is related to the normal vector $\mathbf{n(x)}$ on $\partial\Omega_s$ by

$$\mathbf{N}(\mathbf{x}) = \begin{bmatrix} n_1 & 0 & n_3 \\ 0 & n_3 & n_1 \end{bmatrix},$$

and finally, the matrices $\mathbf{B}^a$ and $\mathbf{P}^a$ are represented by the gradients of the shape functions as

$$\mathbf{B}^a(\mathbf{x}) = \begin{bmatrix} \varphi^a_{,1} & 0 \\ 0 & \varphi^a_{,3} \\ \varphi^a_{,3} & \varphi^a_{,1} \end{bmatrix}, \quad \mathbf{P}^a(\mathbf{x}) = \begin{bmatrix} \varphi^a_{,1} \\ \varphi^a_{,3} \end{bmatrix}.$$

Similarly the normal component of the electric displacement vector $Q(\mathbf{x})$ can be approximated by

$$Q^h(\mathbf{x},\tau) = \mathbf{N}_1(\mathbf{x})\mathbf{G}\sum_{a=1}^{n}\mathbf{B}^a(\mathbf{x})\hat{\mathbf{u}}^a(\tau) - \mathbf{N}_1(\mathbf{x})\mathbf{H}\sum_{a=1}^{n}\mathbf{P}^a(\mathbf{x})\hat{\psi}^a(\tau) - \mathbf{N}_1(\mathbf{x})\mathbf{A}\sum_{a=1}^{n}\mathbf{P}^a(\mathbf{x})\hat{\mu}^a(\tau), \tag{22}$$

where the matrices $\mathbf{G}$, $\mathbf{H}$ and $\mathbf{A}$ are defined in eq. (8) and

$$\mathbf{N}_1(\mathbf{x}) = \begin{bmatrix} n_1 & n_3 \end{bmatrix}.$$

Finally, the density of the magnetic flux $S(\mathbf{x})$ is approximated by

$$S^h(\mathbf{x},\tau) = \mathbf{N}_1(\mathbf{x})\mathbf{R}\sum_{a=1}^{n}\mathbf{B}^a(\mathbf{x})\hat{\mathbf{u}}^a(\tau) - \mathbf{N}_1(\mathbf{x})\mathbf{A}\sum_{a=1}^{n}\mathbf{P}^a(\mathbf{x})\hat{\psi}^a(\tau) - \mathbf{N}_1(\mathbf{x})\mathbf{M}\sum_{a=1}^{n}\mathbf{P}^a(\mathbf{x})\hat{\mu}^a(\tau) \tag{23}$$

with the matrices **R,** **A**and **M** being defined in eq. (9).

Substituting (21)-(23) into the local boundary-domain integral equations (16)-(18), one obtains the following system of ordinary differential equations

$$\sum_{a=1}^{n}\left[\left(\int\limits_{L_s+\Gamma_{st}}\mathbf{N}(\mathbf{x})\mathbf{C}\mathbf{B}^a(\mathbf{x})d\Gamma\right)\hat{\mathbf{u}}^a(\tau)-\left(\int\limits_{\Omega_s}\rho\varphi^a d\Omega\right)\ddot{\hat{\mathbf{u}}}^a(\tau)\right]$$
$$+\sum_{a=1}^{n}\left(\int\limits_{L_s+\Gamma_{st}}\mathbf{N}(\mathbf{x})\mathbf{L}\mathbf{P}^a(\mathbf{x})d\Gamma\right)\hat{\psi}^a(\tau)+$$
$$+\sum_{a=1}^{n}\left(\int\limits_{L_s+\Gamma_{st}}\mathbf{N}(\mathbf{x})\mathbf{K}\mathbf{P}^a(\mathbf{x})d\Gamma\right)\hat{\mu}^a(\tau)=-\int\limits_{\Gamma_{st}}\tilde{\mathbf{t}}(\mathbf{x},\tau)d\Gamma-\int\limits_{\Omega_s}\mathbf{X}(\mathbf{x},\tau)d\Omega, \quad (24)$$

$$\sum_{a=1}^{n}\left(\int\limits_{L_s+\Gamma_{sq}}\mathbf{N}_1(\mathbf{x})\mathbf{G}\mathbf{B}^a(\mathbf{x})d\Gamma\right)\hat{\mathbf{u}}^a(\tau)-\sum_{a=1}^{n}\left(\int\limits_{L_s+\Gamma_{sq}}\mathbf{N}_1(\mathbf{x})\mathbf{H}\mathbf{P}^a(\mathbf{x})d\Gamma\right)\hat{\psi}^a(\tau)-$$
$$-\sum_{a=1}^{n}\left(\int\limits_{L_s+\Gamma_{sq}}\mathbf{N}_1(\mathbf{x})\mathbf{A}\mathbf{P}^a(\mathbf{x})d\Gamma\right)\hat{\mu}^a(\tau)=-\int\limits_{\Gamma_{sq}}\tilde{Q}(\mathbf{x},\tau)d\Gamma+\int\limits_{\Omega_s}\Pi(\mathbf{x},\tau)d\Omega, \quad (25)$$

$$\sum_{a=1}^{n}\left(\int\limits_{L_s+\Gamma_{sb}}\mathbf{N}_1(\mathbf{x})\mathbf{R}\mathbf{B}^a(\mathbf{x})d\Gamma\right)\hat{\mathbf{u}}^a(\tau)-\sum_{a=1}^{n}\left(\int\limits_{L_s+\Gamma_{sb}}\mathbf{N}_1(\mathbf{x})\mathbf{A}\mathbf{P}^a(\mathbf{x})d\Gamma\right)\hat{\psi}^a(\tau)-$$
$$-\sum_{a=1}^{n}\left(\int\limits_{L_s+\Gamma_{sb}}\mathbf{N}_1(\mathbf{x})\mathbf{M}\mathbf{P}^a(\mathbf{x})d\Gamma\right)\hat{\mu}^a(\tau)=-\int\limits_{\Gamma_{sb}}\tilde{S}(\mathbf{x},\tau)d\Gamma, \quad (26)$$

which are applied on the subdomains adjacent to the interior nodes as well as to the boundary nodes on Γ_{st},Γ_{sq} and Γ_{sb}.

The discretized essential boundary conditions for displacements, electrical and magnetic potentials take the form

$$\sum_{a=1}^{n}\varphi^a(\mathbf{x}^b)\hat{\mathbf{u}}^a(\tau)=\tilde{\mathbf{u}}(\mathbf{x}^b,\tau) \text{ for } \mathbf{x}^b\in\partial\Omega_s^b\cap\Gamma_u=\Gamma_{su}^b, \quad (27)$$

$$\sum_{a=1}^{n}\varphi^a(\mathbf{x}^b)\hat{\psi}^a(\tau)=\tilde{\psi}(\mathbf{x}^b,\tau) \text{ for } \mathbf{x}^b\in\partial\Omega_s^b\cap\Gamma_p=\Gamma_{sp}^b, \quad (28)$$

$$\sum_{a=1}^{n} \varphi^a(\mathbf{x}^b)\hat{\mu}^a(\tau) = \tilde{\mu}(\mathbf{x}^b,\tau) \text{ for } \mathbf{x}^b \in \partial\Omega_s^b \cap \Gamma_a = \Gamma_{sa}^b. \tag{29}$$

On the interface Γ_I of the two material layers there are no boundary conditions prescribed but we can guarantee the continuity for the displacements and potentials, as well as the equilibrium for tractions, normal components of the electric displacements and magnetic inductions by collocating the following equations at double nodes $\mathbf{x}^d \in \partial\Omega_s^d \cap \Gamma_I = \Gamma_I^d$

$$\sum_{a=1}^{n^+} \varphi^a(\mathbf{x}^d)\hat{\mathbf{u}}^a(\tau) = \sum_{a=1}^{n^-} \varphi^a(\mathbf{x}^d)\hat{\mathbf{u}}^a(\tau),$$

$$\sum_{a=1}^{n^+} \varphi^a(\mathbf{x}^d)\hat{\psi}^a(\tau) = \sum_{a=1}^{n^-} \varphi^a(\mathbf{x}^d)\hat{\psi}^a(\tau),$$

$$\sum_{a=1}^{n^+} \varphi^a(\mathbf{x}^d)\hat{\mu}^a(\tau) = \sum_{a=1}^{n^-} \varphi^a(\mathbf{x}^d)\hat{\mu}^a(\tau),$$

$$\mathbf{N}(\mathbf{x}^b)\left[\mathbf{C}^+\sum_{a=1}^{n^+}\mathbf{B}^a(\mathbf{x}^b)\hat{\mathbf{u}}^a(\tau)+\mathbf{L}^+\sum_{a=1}^{n^+}\mathbf{P}^a(\mathbf{x}^b)\hat{\psi}^a(\tau)+\mathbf{K}^+\sum_{a=1}^{n^+}\mathbf{P}^a(\mathbf{x}^b)\hat{\mu}^a(\tau)\ -\right.$$

$$\left.-\ \mathbf{C}^-\sum_{a=1}^{n^-}\mathbf{B}^a(\mathbf{x}^b)\hat{\mathbf{u}}^a(\tau)-\mathbf{L}^-\sum_{a=1}^{n^-}\mathbf{P}^a(\mathbf{x}^b)\hat{\psi}^a(\tau)-\mathbf{K}^-\sum_{a=1}^{n^-}\mathbf{P}^a(\mathbf{x}^b)\hat{\mu}^a(\tau)\right]=0, \tag{30}$$

$$\mathbf{N}_1(\mathbf{x}^d)\left[\mathbf{G}^+\sum_{a=1}^{n^+}\mathbf{B}^a(\mathbf{x}^b)\hat{\mathbf{u}}^a(\tau)-\mathbf{H}^+\sum_{a=1}^{n^+}\mathbf{P}^a(\mathbf{x}^b)\hat{\psi}^a(\tau)-\mathbf{A}^+\sum_{a=1}^{n^+}\mathbf{P}^a(\mathbf{x}^b)\hat{\mu}^a(\tau)-\right.$$

$$\left.-\mathbf{G}^-\sum_{a=1}^{n^-}\mathbf{B}^a(\mathbf{x}^b)\hat{\mathbf{u}}^a(\tau)+\mathbf{H}^-\sum_{a=1}^{n^-}\mathbf{P}^a(\mathbf{x}^b)\hat{\psi}^a(\tau)+\mathbf{A}^-\sum_{a=1}^{n^-}\mathbf{P}^a(\mathbf{x}^b)\hat{\mu}^a(\tau)\right]=0, \tag{31}$$

$$\mathbf{N}_1(\mathbf{x}^d)\left[\mathbf{R}^+\sum_{a=1}^{n^+}\mathbf{B}^a(\mathbf{x}^b)\hat{\mathbf{u}}^a(\tau)-\mathbf{A}^+\sum_{a=1}^{n^+}\mathbf{P}^a(\mathbf{x}^b)\hat{\psi}^a(\tau)-\mathbf{M}^+\sum_{a=1}^{n^+}\mathbf{P}^a(\mathbf{x}^b)\hat{\mu}^a(\tau)-\right.$$

$$\left.-\mathbf{R}^-\sum_{a=1}^{n^-}\mathbf{B}^a(\mathbf{x}^b)\hat{\mathbf{u}}^a(\tau)+\mathbf{A}^-\sum_{a=1}^{n^-}\mathbf{P}^a(\mathbf{x}^b)\hat{\psi}^a(\tau)+\mathbf{M}^-\sum_{a=1}^{n^-}\mathbf{P}^a(\mathbf{x}^b)\hat{\mu}^a(\tau)\right]=0, \tag{32}$$

where n^+ and n^- are the numbers of nodes lying in the support domain in medium + and medium -, respectively. The normal vector components in $\mathbf{N}(\mathbf{x}^d)$ and $\mathbf{N}_1(\mathbf{x}^d)$ are taken in the sense of outward normal to the medium +.

The local boundary-domain integral equations (24)-(26) together with the collocation equations (27)-(29) on the global boundary for the essential conditions and tailoring conditions (30)-(32) on the interface are recast into a complete system of ordinary differential equations (ODE)

$$\mathbf{R}\ddot{\mathbf{x}} + \mathbf{F}\mathbf{x} = \mathbf{Y}, \tag{33}$$

where the column-vector $\mathbf{x}$ is formed by the nodal unknowns $\left\{\hat{u}_1^a(\tau), \hat{u}_3^a(\tau), \hat{\psi}^a(\tau), \hat{\mu}^a(\tau)\right\}$.

The Houbolt method (Houbolt, 1950) is applied for the second order ODE (33), in which the "acceleration" is expressed as

$$\ddot{\mathbf{x}}_{\tau+\Delta\tau} = \frac{2\mathbf{x}_{\tau+\Delta\tau} - 5\mathbf{x}_\tau + 4\mathbf{x}_{\tau-\Delta\tau} - \mathbf{x}_{\tau-2\Delta\tau}}{\Delta\tau^2}, \tag{34}$$

where $\Delta\tau$ is the time-step.

Substituting eq. (34) into eq. (33), we get the following system of linear algebraic equations for the unknowns $\mathbf{x}_{\tau+\Delta\tau}$

$$\left[\frac{2}{\Delta\tau^2}\mathbf{R} + \mathbf{F}\right]\mathbf{x}_{\tau+\Delta\tau} = \frac{1}{\Delta\tau^2}5\mathbf{R}\mathbf{x}_\tau + \mathbf{R}\frac{1}{\Delta\tau^2}\left\{-4\mathbf{x}_{\tau-\Delta\tau} + \mathbf{x}_{\tau-2\Delta\tau}\right\} + \mathbf{Y}. \tag{35}$$

4 Numerical results

The following geometrical values for the two-layered composite are considered in the numerical analysis: length $L_x = 16mm$, and thickness of layers $h_e = h_m = 1mm$. For the upper layer with piezoelectric properties we have considered PZT-5A material, where

$$c_{11} = 99.2 \cdot 10^9 Nm^{-2}, \quad c_{13} = 50.778 \cdot 10^9 Nm^{-2},$$

$$c_{33} = 86.856 \cdot 10^9 Nm^{-2}, \quad c_{44} = 21.1 \cdot 10^9 Nm^{-2},$$

$$e_{15} = 12.332 Cm^{-2}, \quad e_{31} = -7.209 Cm^{-2}, \quad e_{33} = 15.118 Cm^{-2},$$

$$h_{11} = 1.53 \cdot 10^{-8} C(Vm)^{-1}, \quad h_{33} = 1.5 \cdot 10^{-8} C(Vm)^{-1}, \quad \rho = 7500 kg/m^3.$$

The bottom layer corresponds to the piezomagnetic $CoFe_2O_4$ material with

$$c_{11} = 286 \cdot 10^9 Nm^{-2}, \quad c_{13} = 170.5 \cdot 10^9 Nm^{-2},$$

$$c_{33} = 269.5 \cdot 10^9 Nm^{-2}, \quad c_{44} = 45.3 \cdot 10^9 Nm^{-2},$$

$d_{15} = 550N(Am)^{-1}, \quad d_{31} = 580.3N(Am)^{-1}, \quad d_{33} = 699.7N(Am)^{-1},$
$\gamma_{11} = 590 \cdot 10^{-6}Wb(Am)^{-1}, \quad \gamma_{33} = 157 \cdot 10^{-6}Wb(Am)^{-1}, \quad \rho = 5500kg/m^3.$

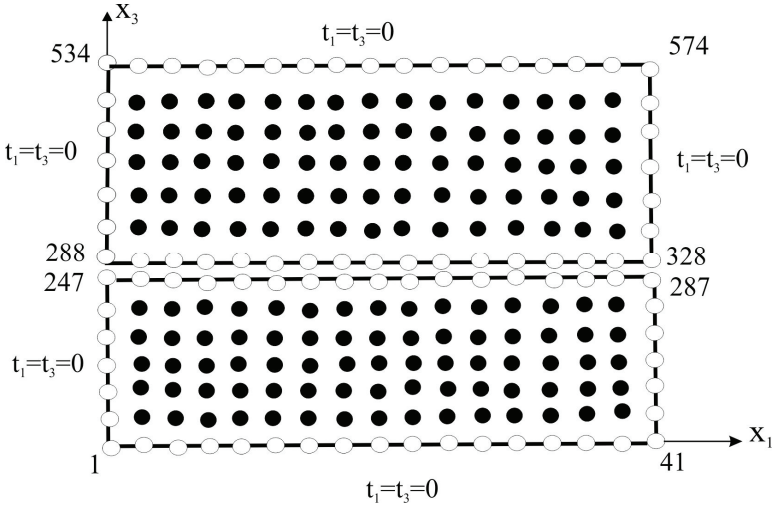

Figure 3: Node distribution and boundary conditions

On the lateral sides vanishing magnetic inductions and electrical displacements are prescribed. The top surface of the piezoelectric layer has vanishing electric displacements and magnetic potential. On the bottom surface of the piezomagnetic layer the magnetic potential -0.1A and a vanishing electric potential are prescribed. The top surface of the piezomagnetic layer and the bottom surface of the piezoelectric layer are perfectly bonded and both magnetic and electric potentials, magnetic flux and electrical displacements are unknown there. The electric potential on the top surface is unknown. We have used 574 (2x41x7) nodes equidistantly distributed for the MLS approximation of the physical quantities (Fig. 3). The local subdomains are considered to be circular with a radius $r_{loc} = 0.0001m$. If the magnetic permeability of the piezoelectric layer is significantly larger than the value of the joined piezomagnetic layer ($\gamma_{11} = 590 \cdot 10^{-6}Wb(Am)^{-1} * 1000$ and $\gamma_{33} = 157 \cdot 10^{-6}Wb(Am)^{-1} * 1000$), the magnetic potential along the thickness of the piezoelectric layer is vanishing as the prescribed value on the top surface. Similarly, if the electric permittivity in the piezomagnetic layer is significantly larger than the value in the piezoelectric layer ($h_{11} = 1.53 \cdot 10^{-8}C(Vm)^{-1} * 1000$ and $h_{33} = 1.5 \cdot 10^{-8}C(Vm)^{-1} * 1000$), the electric potential along the whole piezomagnetic layer is vanishing, like the prescribe quantity on the bottom surface. In the

first numerical analysis the bottom surface of the piezomagnetic layer is clamped, i.e., $u_1 = u_3 = 0$ at $x_3 = 0$. All other composite surfaces are free of tractions.

The computed electric potential on the top surface of the PE layer is presented in Fig. 4. One can observe a quite good agreement between the FEM and the MLPG results. The COMSOL computer code is used for the FEM analyses with 1400 (100x14) linear elements. In the next step, we change the thickness of the piezoelectric layer, while the thickness of the piezomagnetic layer is unchanged. Therefore, we introduce the volumetric ratio of the PE layer as $V_f = h_e/(h_e + h_m)$. One can observe the influence of the volumetric ratio of the PE/PM layers on the electric potential on the top surface of the PE layer in Fig. 5. With increasing PE layer thickness the electric potential on the top surface increases.

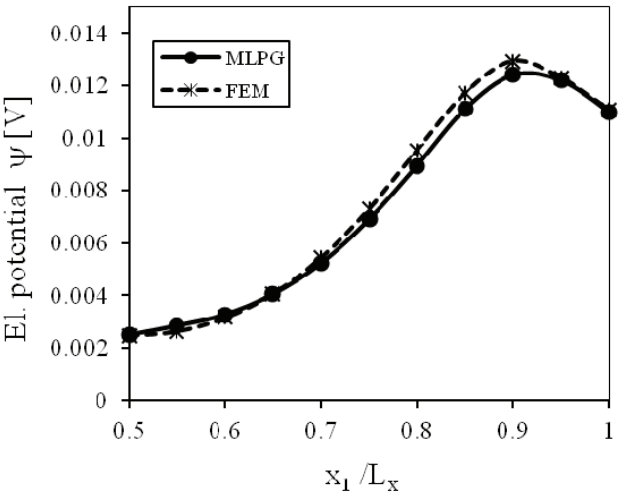

Figure 4: Variation of the electric potential along x_1 on the top surface of PE layer if the bottom of the piezomagnetic layer is clamped

The average intensity of the electric field $\bar{E}_3$ is defined for the composite plate as

$$\bar{E}_3 = \frac{1}{S}\int_S E_3(x_1, x_3)dS, \tag{36}$$

where S is the surface of the two-layered composite in the $x_1 - x_3$ plane. The average magnetic intensity vector is defined similarly. In the considered sample with $h \ll L_x$, the average magnetic intensity can be assessed as $\bar{H}_3 = 0.1A/0.001m =$

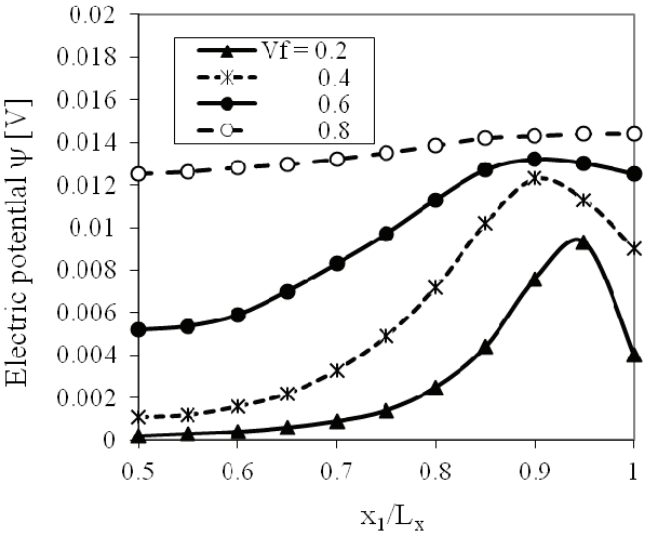

Figure 5: Variation of the electric potential along x_1 on the top surface for various thicknesses of the PE layer

$100A/m$ if $h_e = h_m = 0.001m$. Thus, the ME coefficient under vanishing deformations and polarization can be obtained as $\alpha_{33} = h_{33}\alpha'_{33}$, where $\alpha'_{33} = -\bar{E}_3/\bar{H}_3$ is the ME voltage coefficient (Bichurin et al, 2003). Since both the applied magnetic field and the unknown electric field are oriented along the vertical x_3-direction, it is sometimes reffered to as the out-of-plane longitudinal ME effect (Bichurin et al, 2003) for layered composites.

Pan and Wang (2009) computed the average intensity of the electric field $\bar{E}_3 = \bar{\psi}/(h_e + h_m)$, where $\bar{\psi}$ is the average electric potential on the top surface of the plate. Based on the definition we get the coefficient $\alpha'_{33} = -\bar{E}_3/\bar{H}_3$, where the magnetic intensity $\bar{H}_3 = \mu/h_m$ and $\mu = -0.1A$ on the bottom surface of the PM layer. The variation of the magnetoelectric coefficient versus the volumetric ratio is presented in Fig. 6. One can again observe a very good agreement of the FEM and MLPG results.

In the next example we consider a fixed displacement component $u_3 = 0$ on the bottom surface of the piezomagnetic layer. The variation of the electric potential on the top surface of the PE layer for the volumetric ratio $V_f = 0.5$ is presented in Fig. 7. If we compare the results for clamped and fixed boundary conditions in Figs. 4 and 7, we can see significantly larger electrical potential for fixed boundary conditions. The variations of the electric potentials along x_1 on the top surface of

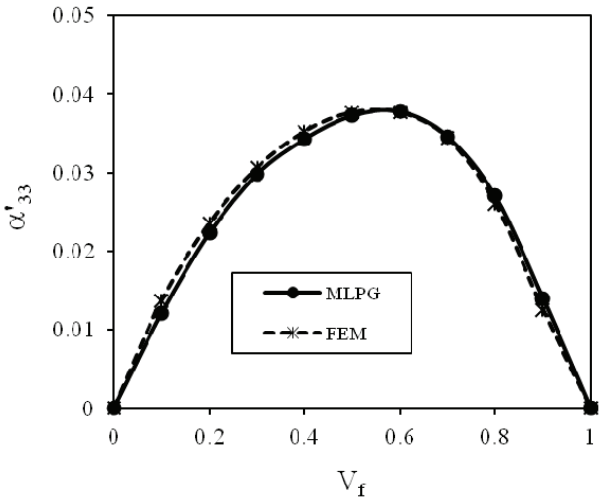

Figure 6: Variation of the magnetoelectric coefficient versus the volumetric ratio for clamped PM layer

the PE layer for various volumetric ratios are given in Fig. 8. The magnetoelectric coefficient for the two-layered PM/PE composite with a fixed displacement $u_3 = 0$ is presented in Fig. 9. One can observe a very good agreement between the present MLPG and the FEM results.

In functionally graded materials (FGMs) the volume fraction of the constituents is varying in a predominant direction. In this paper, we consider an FG piezoelectric layer and a homogeneous piezomagnetic layer. Along the thickness of the PE layer the material properties are continuously varying. An exponential variation of the elastic, piezoelectric and dielectric coefficients is assumed generally as

$$f_{ij}(\mathbf{x}) = f_{ij0} \exp\left[m(x_3 - 0.001)\right], \tag{37}$$

where the symbol f_{ij} is commonly used for particular material coefficients with f_{ij0} corresponding to the material coefficients for PZT-5A. In the numerical analyses, we will use various values of the exponent parameter in order to study the dependence of the ME coefficient on the material gradation along the x_3 direction. Also in this case the displacement $u_3 = 0$ is fixed on the bottom surface of the PM layer. The variation of the electric potential along the x_1 direction on the top surface of the functionally graded PE layer for a fixed homogeneous piezomagnetic layer is presented in Fig. 10. The largest electric potential and the corresponding

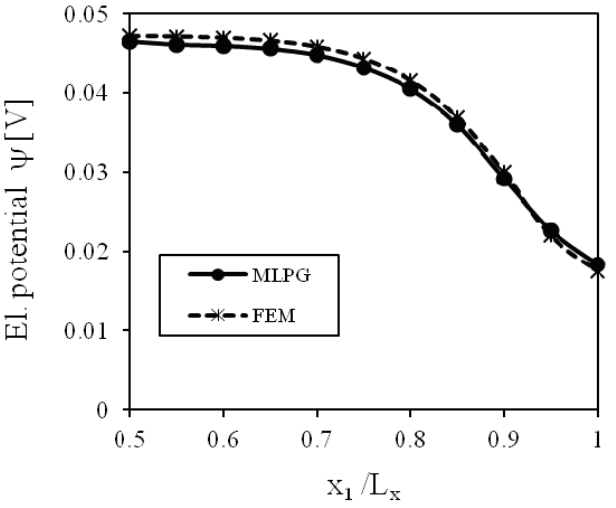

Figure 7: Variation of the electric potential along x_1 on the top surface of PE layer if the bottom of the piezomagnetic layer is fixed $u_3 = 0$ and $V_f = 0.5$

electromagnetic coefficient are observed for a negative exponent m =-1. In such a case all material coefficients of the PE layer have smaller values on the top surface than on the bottom surface. The electric potential is only a little bit larger than that corresponding to the homogeneous layer as presented in Fig. 7. The smallest electric potential corresponds to a positive exponent m =1, valid for all material parameters. If functionally graded properties are considered only for the elastic or the electric material parameters, the electric potential is slightly reduced with respect to the case with both FG elastic and electric parameters. The variation of the ME coefficient with the gradation exponent is presented in Fig. 11.

In previous numerical examples we considered a pure magnetic load on the FG multiferroic laminated composite. In the next example a combined magneto-mechanical load is applied. A uniform mechanical load σ_0 is applied on the top surface of the PE layer. The bottom surface is fixed in the normal direction (u_3=0) but free in the tangential direction. Simultaneously the two-layered plate is subjected a magnetic load with the prescribed magnetic potential $\mu = -0.1A$ on its bottom surface and the vanishing magnetic potential on the top surface. The mechanical load is determined by the non-dimensional parameter $\chi^m = \sigma_0/(d_{33}H_3)$ at a uniform magnetic load $H_3 = 100Am$. One can observe in Fig. 12 that the ME coefficient significantly grows with increasing mechanical load at the constant magnetic load. This phe-

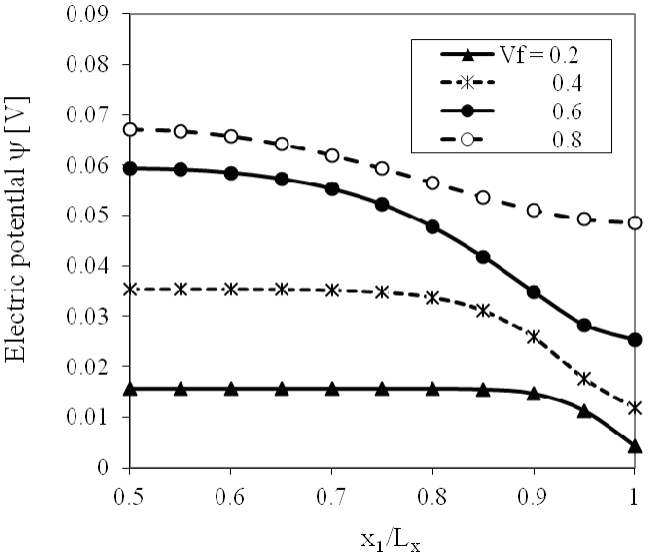

Figure 8: Variation of the electric potential along x_1 on the top surface for various thicknesses of the PE layer if the bottom of the piezomagnetic layer is fixed $u_3 = 0$

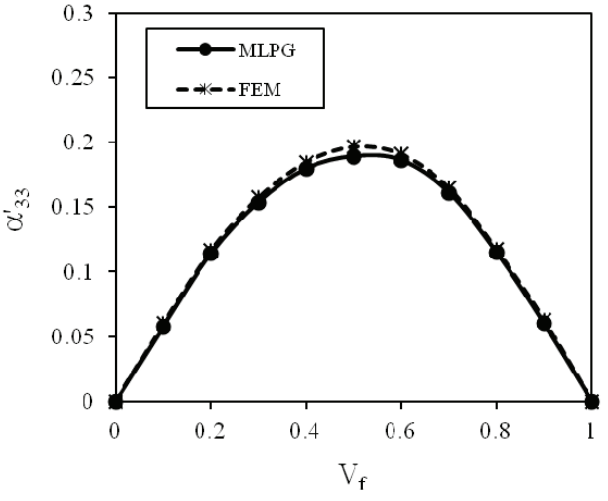

Figure 9: Variation of the magnetoelectric coefficient versus the volumetric ratio if the bottom of the piezomagnetic layer is fixed $u_3 = 0$

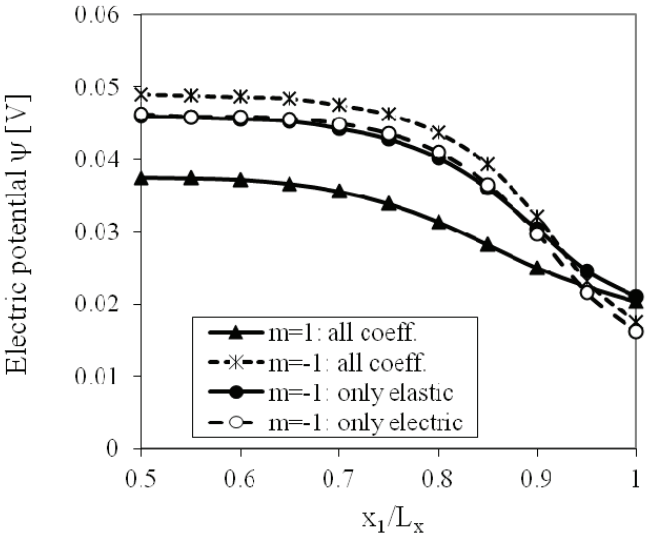

Figure 10: Variation of the electric potential along x_1 on the top surface of functionally graded PE layer if the bottom of the piezomagnetic layer is fixed $u_3 = 0$ and $V_f = 0.5$

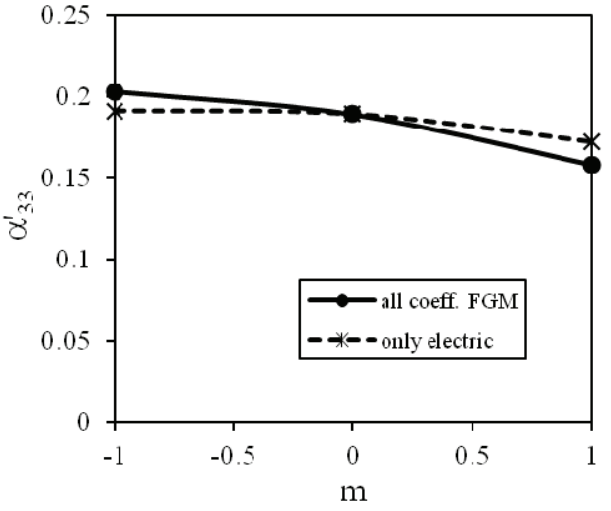

Figure 11: Variation of the ME coefficient with the gradation exponent

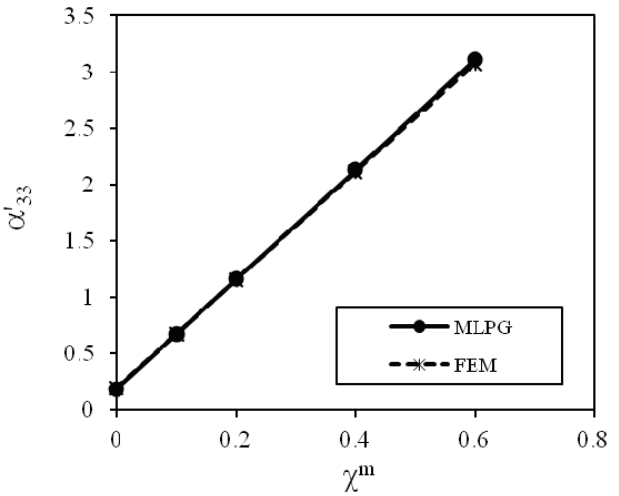

Figure 12: Variation of the magnetoelectric coefficient with the combined load parameter χ^m for two-layered composite with the fixed bottom $u_3 = 0$ and $V_f = 0.5$

nomena can be utilized to enlarge the ME coefficient.

In the next numerical example we analyze the two-layered composite under a combined magneto-mechanical load with an impact mechanical and a constant magnetic load. A uniform mechanical load $\sigma_{33} = 7000Pa$ on the top surface with a Heaviside time variation is considered. It corresponds to $\chi^m = 0.1$. Simultaneously the two-layered composite is subjected to a magnetic load with a prescribed magnetic potential $\mu = -0.1A$ on its bottom surface and a vanishing magnetic potential on the top surface. The bottom surface is fixed in the normal direction (u_3=0) but free in the tangential direction. The geometry and material properties of the plate are the same as in previous examples with static loading conditions. Numerical calculations are carried out for a time-step $\Delta\tau = 0.5 \times 10^{-7}s$. The time variation of the magnetoelectric coefficient is presented in Fig. 13. One can observe a very good agreement of the MLPG and the FEM results for shorter time instants. The magnetoelectric coefficient corresponding to the static loading case, $\alpha_{33}^{stat} = 0,674$, is exceeded significantly in the dynamic loading case.

If the magnetic potential with a Heaviside time variation is applied on the bottom surface of the composite (without mechanical loading) and a finite velocity of elastic waves is considered, the magnetoelectric coefficient is given in Fig. 14. The magnetoelectric coefficient corresponding to the static loading is equal to $\alpha_{33}^{stat} = 0,189$. One can see that the magnetoelectric coefficient is oscillating around

the zero value in the dynamic loading case.

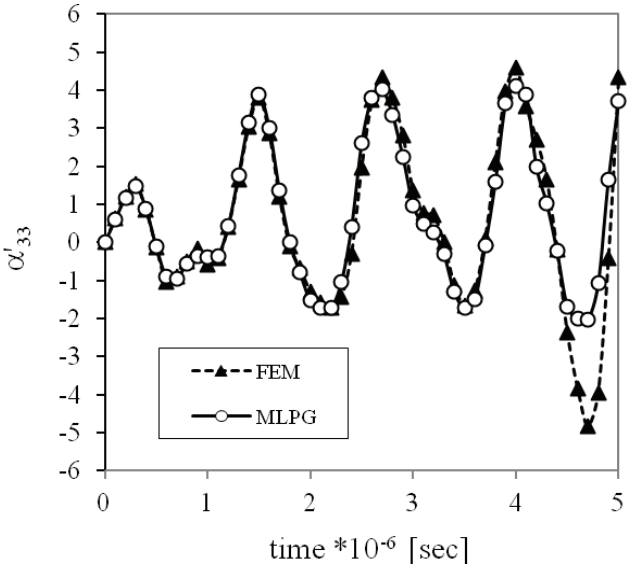

Figure 13: Time variation of the magnetoelectric coefficient for the load parameter $\chi^m = 0.1$

5 Conclusions

After more than a century of theoretical and experimental researches on the ME interaction phenomena the ME effect is now at the cusp of exploitation for device applications. In composite samples the geometrical degrees of freedom have more influences on the ME response than in the case of single-phase compounds. The directions of the applied fields and of the induced ME signal are all perpendicular to the interface of PE and PM layers. The ME voltage coefficient increases with increasing thickness ratio h_m/h_e, between the magnetostrictive and the piezoelectric units because the compressive stress is higher in thinner piezoelectric layers. On the other hand the output voltage, which is the relevant parameter for sensor applications, decreases when h_m/h_e increases.

A meshless local Petrov-Galerkin method (MLPG) is applied to investigate magnetoelectric coefficients for two-layered composite consisting of two dissimilar piezoelectric and piezomagnetic materials. Both static and dynamic loading conditions are considered here. The electric potential in the PE layer is induced by the magnetic potential in the PM layer. The induced electric field is not uniform on the

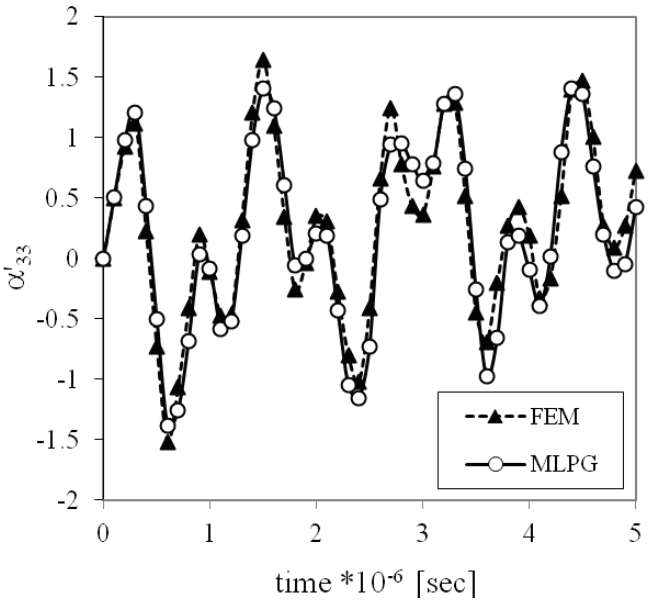

Figure 14: Time variation of the magnetoelectric coefficient for a pure magnetic impact load

top surface of the PE layer. Therefore, the magnetoelectric coefficient is not uniform too. The presented coefficients correspond to the average value of the induced electric potential at the top of the PE layer.

The influences of the exponential variation of the elastic, piezoelectric and dielectric coefficients in the PE layer on the ME coefficient is analyzed in details. The largest electric potential and the corresponding electromagnetic coefficient are observed for a negative exponent m =-1. In this case, all material coefficients of the PE layer have smaller values on the top surface than on the bottom surface.

Acknowledgement: The authors acknowledge the financial supports by the Slovak Science and Technology Assistance Agency registered under number APVV-0014-10 and the German Research Foundation (DFG, Project Nos. ZH 15/14-1 and ZH 15/23-1). The authors also gratefully acknowledge the financial assistance of the European Regional Development Fund (ERDF) under the Operational Programme Research and Development/Measure 4.1 Support of networks of excellence in research and development as the pillars of regional development and support to international cooperation in the Bratislava region/Project No. 26240120020 Building the centre of excellence for research and development of structural com-

posite materials - 2^{nd} stage.

References

Atluri, S.N. (2004): *The Meshless Method, (MLPG) For Domain & BIE Discretizations*, Tech Science Press, Forsyth.

Atluri, S.N., Han, Z.D., Shen, S. (2003): Meshless local Petrov-Galerkin (MLPG) approaches for solving the weakly-singular traction & displacement boundary integral equations. *CMES: Computer Modeling in Engineering & Sciences*, 4, pp. 507-516.

Belytschko, T., Krongauz, Y., Organ, D., Fleming, M., Krysl, P. (1996): Meshless methods: An overview and recent developments. *Comp. Meth. Appl. Mech. Engn.*, 139, pp. 3-47.

Bichurin, M.I., Petrov, V.M., Srinivasan, G. (2003): Theory of low-frequency magnetoelectric coupling in magnetostrictive-piezoelectric bilayers. *Physical Review*, B 68, 054402.

Cordes, L.W., Moran, B. (1996): Treatment of material discontinuity in the element free Galerkin method. *Comput. Meth. Appl. Mech. Engn.*, 139, pp. 75-89.

Dunn, M.L. (1993): Micromechanics of coupled electroelastic composites: effective thermal expansion and pyroelectric coefficients. *Journal of Applied Physics*, 73, pp. 5131-5140.

Eerenstein, W., Mathur, N.D., Scott, J.F. (2006): Multiferroic and magnetoelectric materials. *Nature*, 442, pp. 759-765.

Feng, W.J., Su, R.K.L. (2006): Dynamic internal crack problem of a functionally graded magneto-electro-elastic strip. *Int. J. Solids Structures*, 43, pp. 5196-5216.

Houbolt, J.C. (1950): A recurrence matrix solution for the dynamic response of elastic aircraft. *Journal of Aeronautical Sciences*, 17, pp. 371-376.

Krongauz, Y., Belytschko, T. (1998): EFG approximation with discontinuitous derivatives. *Int. J. Num. Meth. Engn.*, 41, pp. 1215-1233.

Kuo, H.Y. (2011): Multicoated elliptic fibrous composites of piezoelectric and piezomagnetic phases. *Int. Journal of Engineering Science*, 49, pp. 561-575.

Laletin, V.M., Petrov, V.M., Tuskov, D.S., Srinivasan, G. (2008): Frequency dependence of the magnetoelectric effect in ceramic composites based on lead zirconate titanate and nickel ferrite. *Tech. Phys. Lett.*, 34, pp. 83-89.

Milgrom, M., Shtrikman, S. (1994): The magnetoelectric effect of composites and polycrystals. *Ferroelectrics,* 162, pp. 87-91.

Nan, C.W., Bichurin, M.I., Dong, S.X., Viehland, D. (2008): Multiferroic mag-

netoelectric composites: Historical perspective, status, and future directions. *Journal of Applied Physics,* 103031101.

Nan, C.W. (1994): Magnetoelectric effect in composites of piezoelectric and piezomagnetic phases. *Phys. Rev.,* B 50, pp. 6082-6088.

Pan, E., Wang, R. (2009): Effects of geometric size and mechanical boundary conditions on magnetoelectric coupling in multiferroic composites. *Journal of Physics D: Applied Physics,* 42, 245503 (7pp).

Parton, V.Z., Kudryavtsev, B.A. (1988): *Electromagnetoelasticity, Piezoelectrics and Electrically Conductive Solids*. Gordon and Breach Science Publishers, New York.

Ryu, J., Priya, S., Uchino, K., Kim, H.E. (2002): Magnetoelectric effect in composites of magnetostrictive and piezoelectric materials. *J. Electroceramics,* 8, pp. 107-119.

Shastry, S., Srinivasan, G., Bichurin, M.I., Petrov, V.M., Tatarenko, A.S. (2004): Microwave magnetoelectric effects in single crystal bilayers of yttrium iron garnet and lead magnesium niobate-lead titanate. *Phys. Rev.,* B 70, 064416.

Shaulov, A.A., Smith, W.A., Ting, R.Y. (1989): Modified-lead-titanate/polymer composites for hydrophone applications. *Ferroelectrics*, 93, pp. 177-182.

Sladek, J., Sladek, V., Solek, P., Pan, E. (2008a): Fracture analysis of cracks in magneto-electro-elastic solids by the MLPG. *Computational Mechanics*, 42, pp. 697-714.

Sladek, J., Sladek, V., Solek, P., Atluri, S.N. (2008b): Modeling of intelligent material systems by the MLPG. *CMES - Computer Modeling in Engineering & Sciences,* 34, pp. 273-300.

Sladek, J., Sladek, V., Wünsche, M., Zhang, C. (2009): Interface crack problems in anisotropic solids analyzed by the MLPG. *CMES - Computer Modeling in Engineering & Sciences,* 54, pp. 223-252.

Smith, W.A., Shaulov, A.A. (1985): Tailoring the properties of composite piezoelectric materials for medical ultrasonic transducers. *IEEE Ultrasonic Symposium*, 2, pp. 642-647.

Van den Boomgaard, J., Terrell, D.R., Born, R.A.J. (1974): An in situ grown eutectic magnetoelectric composite materials. *Journal of Material Science,* 9, pp. 1705-1709.

Van den Boomgaard, J., Va Run, A.M.J.G., Von Suchtelen, J. (1976): Magnetoelectricity in piezoelectric-magnetostrictive composites. *Ferroelectrics,* 10, pp. 295-298.

Wen, P.H., Aliabadi, M.H. (2008): An improved meshless collocation method for

elastostatic and elastodynamic problems. *Communications in Numerical Methods in Engineering,* 24, pp. 635-651.

Wang, Y., Yu, H., Zheng, M., Wan, J.G., Zhang, M.F., Liu, J.M., Nan, C.W. (2005): Numerical modeling of the magnetoelectric effect in magnetostrictive piezoelectric bilayer. *Applied Physics A*, 81, pp. 1197-1202.

Wood, V.E., Austin, A.E. (1975): in *Proc. Symp. Magnetoelectric Interaction Phenomena in Crystals, Seattle, 1973*, ed. by A.J. Freeman, H. Schmid, Gordon and Breach, New York, p. 181.

Zhai, J.Y., Cai, N., Shi, Z., Lin, Y.H., Nan, C.W. (2004): Coupled magnetoelectric properties of laminated $PbZr_{0.53}Ti_{0.47}O_3/NiFe_2O_4$ ceramics. *J. Appl. Phys*., 95, pp. 5685.